PROCEEDINGS OF SCIENCE

The dRICH detector at the future ePIC experiment

Luisa Occhiuto,[a,*] **P. Antonioli,**[b] **L. Barion,**[c] **F. Bellini,**[d,b] **R.S. Bhadauriya,**[e] **A. Bressan,**[f] **A. Calivà,**[g] **M. Capua,**[a] **C. Chatterjee,**[f] **M. Contalbrigo,**[c] **S. Dalla Torre,**[f] **A. De Caro,**[g] **D. De Gruttola,**[g] **D. Elia,**[h] **S. Fazio,**[a] **T. Ghosh,**[e] **S. Kumar,**[h] **A. Mastroserio,**[i,h] **F. Noferini,**[b] **C. Pecar,**[l] **R. Rath,**[b] **C. Ripoli,**[g] **M. Ruspa,**[m] **E. Tassi,**[a] **S. Vallarino,**[n] **G. Volpe**[o,h] **and A. Vossen**[l]

[a] *Università della Calabria & INFN Gruppo Collegato di Cosenza, Rende (Cosenza), Italy*
[b] *INFN Sezione di Bologna, Italy*
[c] *INFN Sezione di Ferrara, Italy*
[d] *Università di Bologna, Italy*
[e] *M. S. Ramaiah University of Applied Sciences, Bangalore, India*
[f] *Università di Trieste & INFN Sezione di Trieste, Italy*
[g] *Università di Salerno & INFN Gruppo Collegato di Salerno, Italy*
[h] *INFN Sezione di Bari, Italy*
[i] *Università di Foggia, Italy*
[l] *Duke University, Durham, NC, USA*
[m] *Università del Piemonte Orientale & INFN Sezione di Torino, Italy*
[n] *INFN Sezione di Genova, Italy*
[o] *Università di Bari, Italy*

E-mail: luisa.occhiuto@cern.ch

The ePIC detector is designed as a general-purpose detector to enable the entire physics program of the future Electron-Ion Collider (EIC) at BNL, USA.
A key feature will be particle identification (PID). A PID system covering a wide pseudorapidity range [-3.3, 3.5] is critical for accurately separating electrons from hadrons such as pions, kaons, and protons. PID in the forward region will be provided by a dual Radiator Ring Imaging Cerenkov (dRICH) detector. Photons will be focused by spherical mirrors and detected by silicon photomultiplier sensors placed on six spherical tiles.
This contribution aims to provide a concise overview of the dRICH. The latest studies of the achievable pion-kaon separation efficiency will be shown, exploring its dependence on particle momentum and selected pseudorapidity intervals. Furthermore, GEANT4-based simulation studies will be presented, with a particular emphasis on one of the two radiators integrated in the dRICH, the aerogel, which enables a detailed investigation of particle behavior at the low momentum regime. The detector's performance, based on chosen geometries, will also be discussed.

*Speaker

ISSN 1824-8039. Published by SISSA Medialab.

PoS(EPS-HEP2025)513

1. Introduction

The Electron-Ion Collider (EIC) [1] will be the first facility to collide polarized electron and ion beams. The primary goal of the EIC is to explore the dynamics of quantum chromodynamics (QCD), shedding light on the internal structure and the origin of spin and mass of protons and nuclei. A major challenge for the EIC is achieving robust particle identification (PID) [2]. In the proposed ePIC detector, efficient pion, kaon, and proton identification is required across a wide pseudorapidity range ($-3.3 < \eta > 3.5$), demanding more than 3σ K/π separation up to 9, 6, and 50 GeV/c in the backward, central, and forward regions, respectively [3]. To meet these requirements in the forward region, a dual Ring-Imaging Cherenkov (dRICH) detector has been designed, combining two radiators C2F6 gas (n = 1.0008) and aerogel (n = 1.02–1.03). Cherenkov photons will be detected by silicon photomultipliers (SiPMs), which provide single-photon sensitivity, ~50 % photon detection efficiency [4], ~100 ps timing resolution per photon [5], and magnetic field tolerance. However, SiPMs are subject to dark current and dark count rate (DCR) noise, potentially worsened by radiation damage [6]. The photosensors, covering a total area of ~3m^2, will be mounted on six spherical tiles and coupled to six focusing mirrors, as shown in Figure 1.

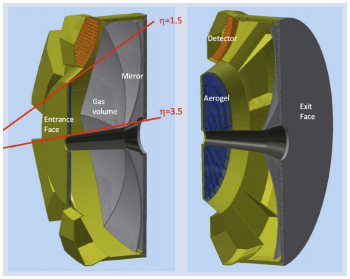

(a) 3D mechanical model of the dRICH apparatus.

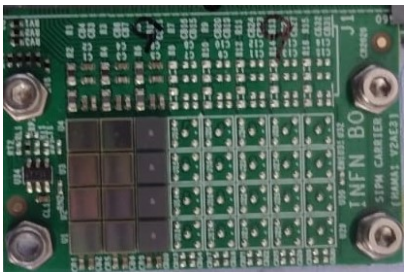

(b) SiPM board.

Figure 1: dRICH schematic on the left and SiPM board on the right.

Given the moderate radiation environment expected during operation, evaluating the radiation hardness of the SiPMs is essential. Simulations indicate that the neutron-equivalent fluence at the dRICH photosensor plane will be approximately $\sim 1-5\times10^7$ particles/cm^2 per fb^{-1} of integrated luminosity. Assuming a collection of 100 fb^{-1} of integrated luminosity, the cumulative fluence may reach $\lesssim 10^{10}$ particles/cm^2 [7]. To maintain dark count rates below 100 kHz/mm^2, SiPMs must operate at low temperatures, while periodic thermal treatments can mitigate radiation-induced degradation. The characterization campaign employed a test matrix comprising three rows, each equipped with a different SiPM model: four Hamamatsu S13360-3050 units [4], four S13360-3075 sensors [4], and four S14160-3050 devices [8].

2. Performance studies

The operation principle of the dRICH relies on the emission of Cherenkov radiation [9], produced when a charged particle traverses a medium at a velocity exceeding the phase velocity of

light in that medium. The emitted photons can be collected and analyzed to extract the particle's velocity; combined with the momentum information provided by the ePIC spectrometer, this allows for the determination of the particle mass. The required Cherenkov angle resolution for achieving different levels of pion–kaon separation, expressed in terms of standard deviations, is illustrated in Fig. 2. Three scenarios are considered: the nominal case with a refractive index of n = 1.02, an alternative evaluation with n = 1.026, and a case with n = 1.03. Optical optimization has been carried out specifically for the most demanding kinematic region of $\eta > 2.5$.

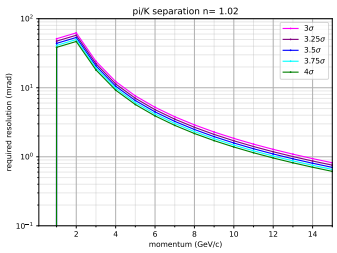

(a) Required Aerogel resolution with n=1.02.

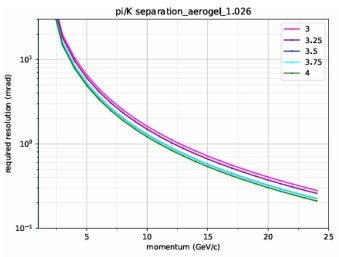

(b) Required Aerogel resolution with n=1.026.

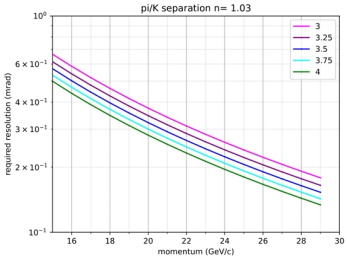

(c) Required Aerogel resolution with n=1.03.

Figure 2: Required resolution for a given π/K separation for aerogel.

Figure 3 shows $N\sigma$ separation as a function of momentum, for both aerogel and gas radiators, across three different pseudorapidity ranges.

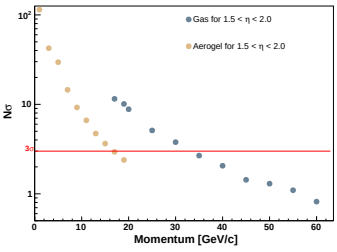

(a)

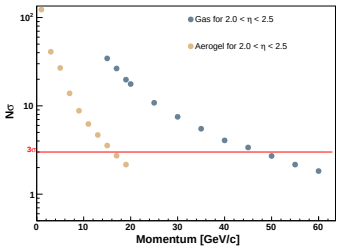

(b)

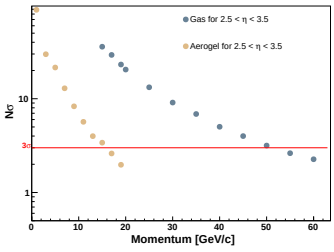

(c)

Figure 3: Nσ separation in different pseudorapidity ranges.

It is observed that a separation larger than 3σ is achieved up to about 15 GeV/c for aerogel, while for gas such separation can be reached up to 50 GeV/c. Fixing $\eta = 2.0$, we observed that we achieve a 3σ separation at $\sim$ 17 GeV/c with a refractive index of n=1.03, as shown in Fig. 4, with overall results similar to those obtained for n=1.026.

Subsequent studies were carried out to assess the non-negligible contribution of chromatic aberration in this context. Chromatic aberration is an optical phenomenon that affects the precision with which the Cherenkov angle can be measured. It arises because the refractive index of the radiator medium (aerogel or gas) depends on the wavelength of light. This introduces a systematic uncertainty in the determination of the Cherenkov angle. Chromatic aberration is identified as the dominant source of angular resolution degradation per photon [10], see Fig. 5(a).

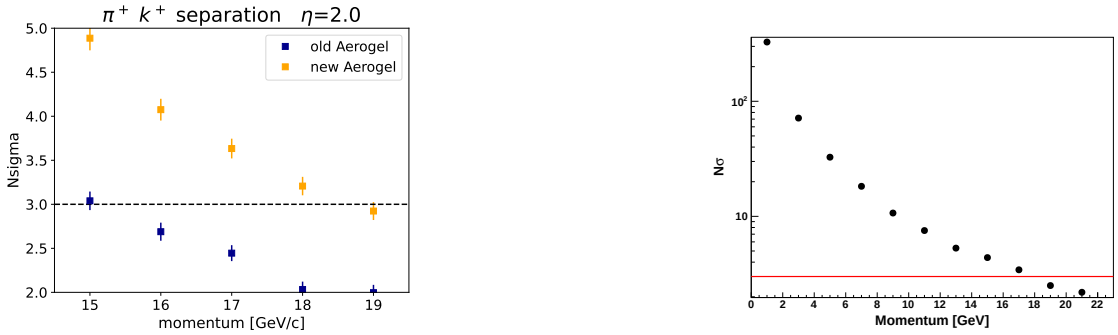

(a) **(b)**

Figure 4: **(a)** Nσ separation for n=1.02 (old Aerogel), n=1.026 (new Aerogel), **(b)** n=1.03 at fixed η = 2.0.

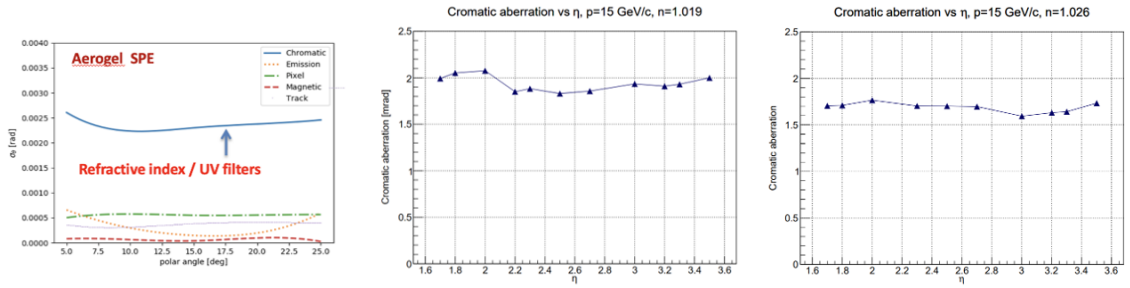

(a) **(b)** **(c)**

Figure 5: **(a)** Contributions to the single-photon angular resolution for aerogel, **(b)** Chromatic aberration at fixed momentum 15 GeV/c for n = 1.019, **(c)** Chromatic aberration at fixed momentum 15 GeV/c for n = 1.026

To quantify the impact of this effect on the single-photon resolution, dedicated simulations were performed assuming both a fixed refractive index and a wavelength-dependent refractive index λ. A total of 1000 pion events were generated with a fixed momentum of 15 GeV/c, covering different pseudorapidity ranges. All simulations were repeated for two distinct values of the refractive index, n = 1.019 and n = 1.026. The results, presented in Fig. 5, show that for an aerogel with a refractive index of n = 1.019 and a particle momentum of 15 GeV/c, the chromatic aberration remains essentially constant across the η range, with a typical value of about 2 mrad. This observation indicates that, at least in this configuration, chromatic dispersion does not significantly worsen with increasing incidence angle. At first glance, it might appear counterintuitive that this material exhibits a lower chromatic aberration than that with n = 1.026, since one might expect that a smaller refractive index would automatically correspond to reduced dispersion and, therefore, to lower chromatic aberration. In reality, however, what determines the magnitude of the effect is not the average value of n itself, but rather how strongly the refractive index varies with the wavelength of light.

The optimization of the aerogel geometry, previously modeled as a single solid block, involves the development of a dedicated support structure, ideally in carbon fiber, to ensure stable positioning within a rigid mechanical frame. A modular structure has been implemented (Fig. 6), based on

mathematical considerations, allowing most key parameters to be adjusted via an XML file.

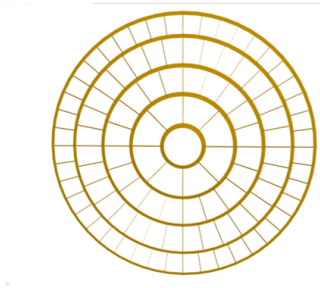

(a)

Figure 6: New support structure in carbon fiber.

This approach eliminates the need for direct source code modifications, enhancing the configurability and flexibility of the setup. Simulation tests were performed to evaluate the variation in acceptance before and after the introduction of the aerogel support structure (Fig.7). These studies

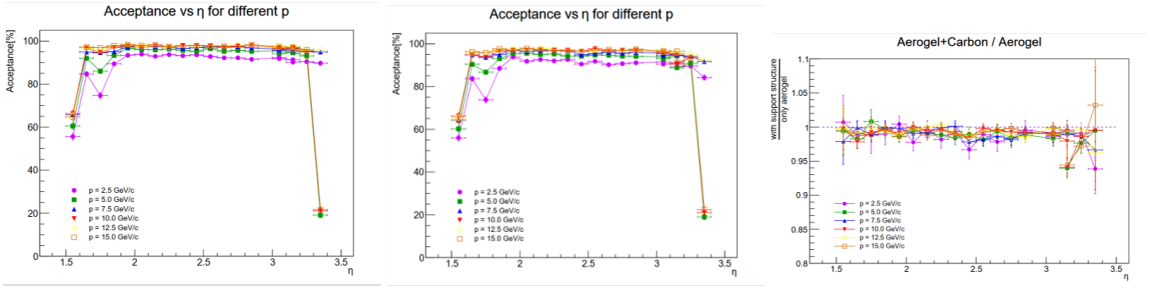

(a) **(b)** **(c)**

Figure 7: **(a)** Acceptance without carbon fiber structure, **(b)** Acceptance with carbon fiber structure, **(c)** Ratio between Acceptance without carbon fiber structure and Acceptance with carbon fiber structure

were carried out using pions, over different ranges of pseudorapidity and momentum, and for the aerogel with a refractive index of n = 1.019. To confirm that no significant changes occur, the ratio between the two configurations was computed. As shown in Fig. 7, the maximum loss in acceptance is approximately 4-5% at high pseudorapidity values.

3. Conclusions

The dRICH detector will provide the ePIC experiment with precise particle identification (PID) capabilities in the forward endcap region, corresponding to the direction of the outgoing hadron beam. Performance studies indicate that the dRICH can achieve a 3σ π/K separation for momenta extending slightly beyond 50 GeV/c in this region. The aerogel radiator with a refractive index of n = 1.026 demonstrates improved 3σ resolution relative to the baseline refractive index configuration. Chromatic aberration has been identified as the dominant source of per-photon angular resolution degradation. In parallel, a dedicated simulation framework is being developed to implement a carbon-fiber support structure, aimed at accurately modeling the aerogel segmentation while maintaining high geometrical acceptance.

Bibliography

[1] A. Accardi et al., "Electron Ion Collider: The Next QCD Frontier", *Eur. Phys. J. A* **52** (2016) no.9, 268 [arXiv:1212.1701].

[2] T. Ullrich, "Requirements and R&D for detectors at the future Electron–Ion Collider," *Nucl. Instrum. Meth. A*, vol. 1039, p. 167041, 2022. doi: 10.1016/j.nima.2022.167041

[3] R. Abdul Khalek *et al.*, "Science Requirements and Detector Concepts for the Electron–Ion Collider: EIC Yellow Report," *Nucl. Phys. A*, vol. 1026, p. 122447, 2022. doi: 10.1016/j.nuclphysa.2022.122447

[4] Hamamatsu Photonics, "S13360 Series," https://www.hamamatsu.com/content/dam/hamamatsu-photonics/sites/documents/99_SALES_LIBRARY/ssd/s13360_series_kapd1052e.pdf

[5] C. Betancourt, A. Dätwyler, P. Owen, A. Puig, and N. Serra, "SiPM single photon time resolution measured via bi-luminescence," *Nucl. Instrum. Meth. A*, vol. 958, p. 162851, 2020. doi: 10.1016/j.nima.2019.162851

[6] E. Garutti and Yu. Musienko, "Radiation damage of SiPMs," *Nucl. Instrum. Meth. A*, vol. 926, pp. 69–84, 2019.

[7] R. Preghenella *et al.*, "Study of radiation effects on SiPM for an optical readout system for the EIC dual-radiator RICH," *Nucl. Instrum. Meth. A*, vol. 1056, p. 168578, 2023.

[8] Hamamatsu Photonics, "S14160/S14161 Series," https://www.hamamatsu.com/content/dam/hamamatsu-photonics/sites/documents/99_SALES_LIBRARY/ssd/s14160_s14161_series_kapd1064e.pdf

[9] E. Nappi and J. Seguinot, "Ring Imaging Cherenkov Detectors: The state of the art and perspectives," *La Rivista del Nuovo Cimento*, vol. 28, pp. 1–130, 2005.

[10] S.Dalla Torre, "EIC preTDR – Chapters 2 and 8, DRAFT, Version 1," Zenodo, 2024. doi: 10.5281/zenodo.14328280 https://eicweb.phy.anl.gov/EIC/juggler